Human Molecular Genetics, 2009, Vol. 18, No. 24 ***4711–4723***
doi:10.1093/hmg/ddp434
Advance Access published on September 14, 2009

Nephrocystin-1 and nephrocystin-4 are required for epithelial morphogenesis and associate with PALS1/PATJ and Par6

Marion Delous[1,2,†], Nathan E. Hellman[1,2,3,†], Helori-Maël Gaudé[1,2], Flora Silbermann[1,2], André Le Bivic[4], Rémi Salomon[1,2,5], Corinne Antignac[1,2,6] and Sophie Saunier[1,2,*]

[1]INSERM, U-574, Hôpital Necker-Enfants Malades, Paris, France, [2]Université Paris Descartes, Paris, France, [3]Nephrology Division, Massachusetts General Hospital, Charlestown, MA, USA, [4]CNRS UMR6216, Equipe labellisée LNCC, IBDML, Faculté des Sciences de Luminy, Marseille, France, [5]AP-HP, Pediatric Nephrology and [6]AP-HP, Department of Genetics, Hôpital Necker-Enfants Malades, Assistance Publique–Hôpitaux de Paris, Paris, France

Received July 13, 2009; Revised and Accepted September 8, 2009

Nephronophthisis (NPH) is an autosomal recessive disorder characterized by renal fibrosis, tubular basement membrane disruption and corticomedullary cyst formation leading to end-stage renal failure. The disease is caused by mutations in *NPHP1-9* genes, which encode the nephrocystins, proteins localized to cell–cell junctions and centrosome/primary cilia. Here, we show that nephrocystin mRNA expression is dramatically increased during cell polarization, and shRNA-mediated knockdown of either *NPHP1* or *NPHP4* in MDCK cells resulted in delayed tight junction (TJ) formation, abnormal cilia formation and disorganized multi-lumen structures when grown in a three-dimensional collagen matrix. Some of these phenotypes are similar to those reported for cells depleted of the TJ proteins PALS1 or Par3, and interestingly, we demonstrate a physical interaction between these nephrocystins and PALS1 as well as their partners PATJ and Par6 and show their partial co-localization in human renal tubules. Taken together, these results demonstrate that the nephrocystins play an essential role in epithelial cell organization, suggesting a plausible mechanism by which the *in vivo* histopathologic features of NPH might develop.

INTRODUCTION

Nephronophthisis (NPH) is an autosomal recessive, chronic tubulointerstitial nephropathy that represents the most common genetic cause of end-stage renal disease in children and adolescents. Disease onset typically begins as a urine concentrating defect during the first decade of life and is followed by a progressive deterioration of renal function. Histological lesions in NPH are characterized by tubular atrophy with thickened tubular basement membranes, diffuse interstitial fibrosis and, at a later stage, the development of cysts at the cortico-medullary junction. Nine disease genes (*NPHP1-9*) have been identified to date. The corresponding proteins encoded by the *NPHP* genes, the nephrocystins, are ubiquitously expressed in the kidney, brain and eye, and their function is still being determined. At a subcellular level, the nephrocystins have been localized to a variety of sites, being found at cell–cell junctions, centrosomes and primary cilia of renal epithelial cells, leading to speculation that the nephrocystins may have different functions at these various sites. The primary cilium is a sensory organelle found in almost all cell types in mammals that is assembled as an extension of the centriole-derived basal body. In renal tubular cells, cilia are localized to the apical membrane where they are hypothesized to function as flow mechanosensors that regulate the cell cycle and epithelial differentiation. The critical importance of cilia in human cystic kidney disorders has been emphasized by the observation that virtually

*To whom correspondence should be addressed at: Inserm U574, Tour Lavoisier, Hôpital Necker-Enfants Malades, 149, rue de Sèvres, 75015 Paris, France. Tel: +33 144495099; Fax: +33 144490290; E-mail: sophie.saunier@inserm.fr
†The authors wish it to be known that, in their opinion, the first two authors should be regarded as joint First Authors.

all proteins associated with cystic kidney diseases, including autosomal dominant polycystic kidney disease, NPH, Bardet–Biedl, oro-facio-digital, Joubert and Meckel–Gruber syndromes, are localized to the cilia (reviewed in 1). The variety of extrarenal symptoms associated with cystic kidney diseases, such as retinal dystrophy, cerebellar hypoplasia, mental retardation, situs inversus, polydactyly and hepatic cysts would seem to implicate cilia in multiple diverse developmental processes.

However, nephrocystins are not exclusively localized to the primary cilia, and several studies have pointed out a possible role for nephrocystin-1, nephrocystin-4 and inversin in the regulation of cell–cell adhesion. Our group and others have shown that these nephrocystins interact with one another, forming a nephrocystin complex (2–7) which simultaneously interacts with signaling proteins involved in the regulation of cell adhesion, such as p130Cas, Pyk2, ACK, and with proteins associated directly with the microtubular and actin cytoskeleton, such as tensin and filamins (8–12). This is consistent with their subcellular localization at cell–cell junctions in polarized MDCK cells (2,9,11) and suggests a possible role for the nephrocystins in cytoskeletal organization and establishment or maintenance of cell polarity. The proper sorting of proteins to unique apical and basolateral plasma membrane compartments has been shown to be a critical principle in kidney development and homeostasis (13).

In order to better understand the relationship of nephrocystins to primary cilia and epithelial organization, we studied MDCK cell lines in which the expression of *NPHP1* and *NPHP4* genes has been reduced by shRNA. We chose to focus on *NPHP1* and *NPHP4*, whose protein products have been shown to localize to both primary cilia and cell adhesion junctions and to interact with cell adhesion protein complexes.

RESULTS

NPHP genes are upregulated during cell polarization of MDCK cells

In an initial attempt to determine the function of nephrocystins in relation to epithelial cell polarity and cilia formation, we analyzed the expression of *NPHP* genes in a time-course experiment, as ciliated MDCK cells developed into well-polarized epithelial monolayers. Interestingly, the expression of *NPHP1* and *NPHP4* was upregulated ~6-fold in fully polarized MDCK cells compared with the expression level at low confluence (day 2) (Fig. 1A). Similarly, the expression of other *NPHP* genes, *NEK8/NPHP9*, *GLIS2/NPHP7*, *NPHP3*, *RPGRIP1L/NPHP8* and *INVS/NPHP2* increased between 2.5- and 11-fold. In contrast, the expression of *CEP290/NPHP6*, whose protein product CEP290/nephrocystin-6 has been suggested to play a role in centrosomal function, stayed relatively constant as cells underwent polarization. The expression of other ciliary genes such as *PKHD1* and *IFT88* was also upregulated during the establishment of cell polarity, whereas the expression of genes encoding other centrosomal proteins, like ninein and pericentrin, was unchanged similar to the expression pattern of *CEP290/NPHP6* (Supplementary Material, Fig. S1). This increased expression of *NPHP1* and *NPHP4* during cell polarization is consistent with the dynamic subcellular localization of these proteins according to the degree of epithelial confluence. For instance, we have previously shown that nephrocystin-4 localizes to the cytoplasm and microtubule-organizing center in subconfluent MDCK cells but co-localizes with β-catenin at cell–cell contacts in well-polarized cells (11). Similarly, the localization of nephrocystin-1 in respiratory epithelial cells has been shown to shift from the cytoplasm to the ciliary transition zone during respiratory epithelial cell polarization (14).

NPHP knockdown cells do not present obvious polarity defects but exhibit abnormal cilia in cultured monolayers

In order to examine whether loss-of-function of either nephrocystin-1 or nephrocystin-4 leads to abnormal apico-basal polarity or abnormal cilia formation, we generated stable *NPHP1* and *NPHP4* knockdown MDCK cell lines (N1-KD and N4-KD, respectively). Silencing of *NPHP1* and *NPHP4* was achieved by RNA interference using the lentiviral vector pSICOR to stably express shRNA along with a GFP reporter (15) (Fig. 1B), which led to a residual *NPHP1* and *NPHP4* expression of 21 and 17%, respectively, compared with empty vector control cell lines as assessed by quantitative RT–PCR (Fig. 1C). In addition, western blotting using an antibody against nephrocystin-1 confirmed a similar decrease in protein levels in N1-KD cell lines (Supplementary Material, Fig. S2A); we were unable to detect endogenous nephrocystin-4 using currently available antibodies. Of note, although N4-KD cell lines exhibited a decrease in *NPHP4* and *NPHP1* expression as determined by qPCR analysis, suggesting that their transcriptional regulation may be linked, there was no detectable decrease in nephrocystin-1 protein by Western blot (Supplementary Material, Fig. S2A). As the level of *NPHP* extinction varied among different populations of transduced cells, clonal cell lines were established, which demonstrated a range of *NPHP1* expression between 11 and 23% of control levels for five N1-KD clones, and *NPHP4* expression between 5 and 45% of controls for seven N4-KD clones (Supplementary Material, Fig. S2B). The following experiments were performed using clonal cell lines with the greatest degree of gene extinction.

We first performed immunostaining of apico-basal markers such as the apical surface protein gp135, the tight junctional protein, occludin, and the basolateral protein, E-cadherin, on control and *NPHP*-deficient MDCK cell lines grown for 7 days on transwell filters. No obvious defects were observed in *NPHP*-deficient cell lines, as gp135, occludin and E-cadherin were appropriately localized at the apical surface, the tight junctions (TJs) and the lateral membrane, respectively (Fig. 2). We then analyzed primary cilia formation of cells grown as epithelial monolayers as assessed by immunostaining with acetylated-α-tubulin (Fig. 3A) and determined the number and the length of the cilia in N1-KD and N4-KD clonal cell lines. Although most (>80%) control cells were found to have a primary cilium, only 65% of N1-KD clonal cells contained cilia ($P < 0.05$) (Fig. 3B, upper panel). N4-KD clonal cell lines, in contrast, did not show any defect in ciliated cell number; however, the length of the cilia in both N1-KD and N4-KD clonal cell lines was shorter than in control cells with 61 and 69% of cilia smaller than 2 μm,

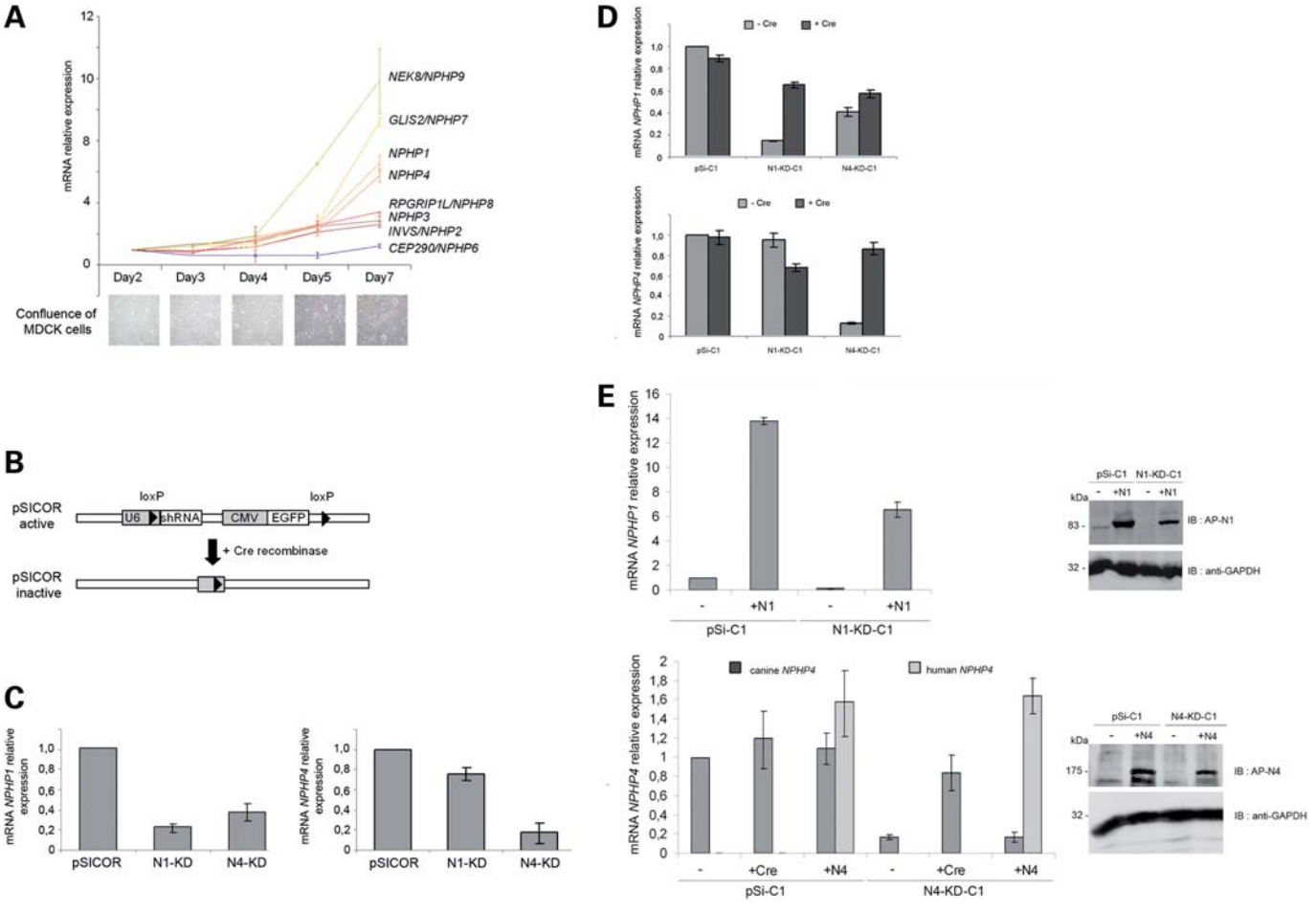

Figure 1. *NPHP* gene expression during cell polarization and generation of *NPHP* knockdown, Cre- and cDNA-rescued MDCK cell line. (**A**) Quantitative RT–PCR analysis of *NPHP* gene expression during time-course experiments performed on MDCK cells. Confluence of cells at each time point is shown by light microscopy pictures. (**B**) Scheme of the lentiviral pSICOR-GFP vector. (**C**) Quantitative RT–PCR analysis of *NPHP1* (left panel) and *NPHP4* (right panel) gene expression in polyclonal control pSICOR, N1-KD and N4-KD cell lines. (**D**) Quantitative RT–PCR analysis of *NPHP1* (upper panel) and *NPHP4* (lower panel) gene expression in a clonal cell population before and after the addition of Cre recombinase. (**E**) Quantitative RT–PCR and western blot analysis of human *NPHP1* and *NPHP4* cDNA expression, introduced by lentiviral infection in knockdown cell lines. *NPHP1* primers for quantitative RT–PCR were homologous to both human and canine sequences, whereas two sets of primers specific to human or canine *NPHP4* sequences were used. GAPDH protein level was used as protein-loading control.

respectively, compared with only 3% in control cell lines (Fig. 3B, lower panel).

To confirm that abnormal cilia formation was due to the loss of *NPHP1* and *NPHP4* expression, we restored the expression of *NPHP* genes by excising the shRNA and GFP-containing cassette using adenoviral Cre recombinase (Fig. 1B). *NPHP* gene expression was partially restored to 65% of control levels for *NPHP1* and to 86% of control levels for *NPHP4* in Cre-infected populations of N1-KD and N4-KD clonal cell lines, respectively (Fig. 1D). In addition, we performed rescue experiments in which human *NPHP1* or *NPHP4* cDNA was expressed in MDCK knockdown clonal cell lines (Fig. 1E). Strategies of both *NPHP1* and *NPHP4* expression restoration allow a rescue of the cilia phenotype. Indeed, the number of ciliated cells in N1-KD cell line was partially reinstated with 71% (Cre rescue) and 77% (cDNA rescue) of cells exhibiting a primary cilium (Fig. 3C, upper panel). The length of cilia was greatly improved with no more than 20% of cilia smaller than 2 μm in both rescued N1-KD and N4-KD cell lines (Fig. 3C, lower panel), indicating that the number of ciliated cells and the cilia length defects were mediated via shRNA-specific knockdown of the targeted nephrocystins. These data are consistent with the hypothesis that both nephrocystin-1 and nephrocystin-4 play some role in primary cilia formation.

NPHP knockdown MDCK cell lines exhibit delayed TJ formation

Even though there was no obvious defect in apico-basal cell polarity in N1-KD and N4-KD cell lines when grown as monolayers over 7 days, we sought to determine whether there were more subtle defects in the establishment of cell polarity by performing a calcium switch experiment. Control, N1-KD and N4-KD clonal cells grown to confluence over 7 days were incubated overnight in low-calcium media to dissociate cell–cell contacts and abolish apico-basal polarity. The following day, normal growth medium

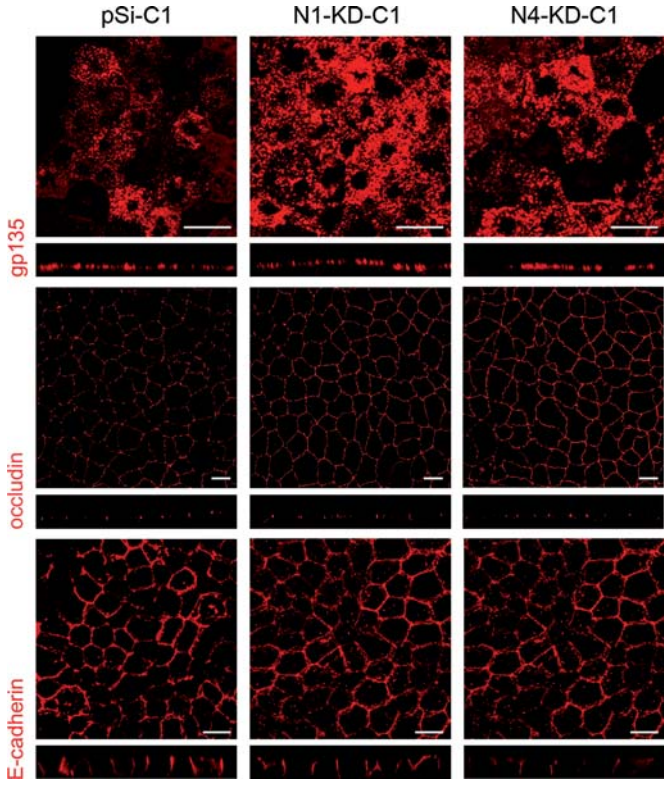

Figure 2. No obvious polarity defects in *NPHP* knockdown cells. Immunostaining of the apical gp135 protein, the TJ protein occludin and the baso-lateral marker E-cadherin was performed on MDCK cells grown on transwell filters for 7 days. Scale bars are 10 μm.

(containing calcium) was added to allow the re-formation of TJs and restoration of cell–cell contacts. TJ formation was assessed by immunostaining of the TJ marker protein, ZO1. In control cell lines, ZO1 was observed to localize to apical regions of cell–cell contacts correlating with TJs as early as 1 h after calcium switch and was completely recruited to these regions within 3 h. In contrast, there was a delay in the formation of TJs in N1-KD and N4-KD cells, as ZO1 was not localized to TJs 1 h after exposure to normal growth medium (Fig. 4A). In parallel with ZO1 staining, the transepithelial electrical resistance (TER) was measured after the addition of normal medium in both control and *NPHP*-deficient cell lines at various time points. Whereas the TER of control cell line increased rapidly to reach a maximum value of 1000 Ωcm^2 at 4 h following the addition of calcium, the N1-KD and N4-KD cell lines showed a markedly delayed increase in TER along with a decreased maximum TER value (Fig. 4B). In four independent experiments, N4-KD clonal cell lines showed a consistently pronounced TER delay, whereas N1-KD clonal cell lines showed a milder and more variable TER delay. Both the rate of TER increase following calcium switch and the appearance of ZO1 staining to TJs 1 h after calcium switch were restored to control levels in Cre-infected N1-KD and N4-KD MDCK cells (Fig. 4B) as well as human cDNA-rescued cell lines (Fig. 4C). Taken together, these results indicate that nephrocystins-1 and -4 are required for the proper timing of tight junctional establishment necessary for the formation of a fully polarized epithelial monolayer.

NPHP knockdown MDCK cells grown in three-dimensional culture demonstrate disorganized, multi-lumen cyst formation

To further examine the potential role for the nephrocystins in the establishment of apico-basal polarity and epithelial architecture, we sought to observe the growth of N1-KD and N4-KD MDCK cell lines in a three-dimensional (3D) type I collagen matrix. When grown in such a matrix, MDCK cells spontaneously form well-organized, hollow multi-cellular structures with a single lumen after 3 weeks' growth, referred to as 'cysts' (16). These cysts demonstrate a clear apico-basal polarity with a basement membrane surrounding the basolateral surface of the cyst and primary cilia extending into the apical cyst lumen, providing a more physiologic model of epithelial cell polarity than cells grown in standard 2D cell culture models. Interestingly, depletion of either nephrocystin-1 or nephrocystin-4 in MDCK cell lines led to severely disorganized structures containing multiple lumens when grown in type-I collagen compared with control MDCK cell lines which formed organized, single-lumen structures (Fig. 5A). Approximately 60 and 40% of polyclonal N1-KD and N4-KD cell cysts, respectively, displayed an abnormal, multi-lumen phenotype; in contrast, the large majority (80%) of control cysts contained a single lumen (Fig. 5B). In addition, several monoclonal cell lines were subjected to morphologic analysis in similar 3D collagen growth experiments. All the three monoclonal control cell lines selected displayed a normal, single-lumen phenotype, whereas four out of the five N1-KD clones and six out of the seven N4-KD clones (all of which had approximately the same levels of gene knockdown) had predominantly multi-lumen cysts with a mean of 85 and 92% of abnormal cysts, respectively (Fig. 5C). The difference observed in the proportion of abnormal cysts between polyclonal and clonal cell lines is probably due to the greater and more homogeneous knockdown of the *NPHP* genes in the clonal cell lines. Three-dimensional culture of Cre-infected N1-KD and N4-KD cells demonstrated partial rescue of the multi-lumen phenotype, as 64 and 57% of cysts were normal with a single lumen (Fig. 5D). Similarly, a partial restoration of the 3D phenotype could be observed with cDNA-rescued cell lines, despite a slightly less efficient rescue of 33% of single-lumen cysts observed for N1-KD and 61% for N4-KD cell lines (Fig. 5D), demonstrating that the 3D growth defect was indeed due to nephrocystin deficiency. This abnormal, multi-lumen phenotype observed in *NPHP* knockdown cell lines might be explained by the fact that these cells exhibit abnormally increased proliferation. However, *NPHP* knockdown cells showed a similar growth rate compared with control cell lines in 2D culture, using a colorimetric quantification of living cells (Supplementary Material, Fig. S3), making this explanation less likely.

We then analyzed the polarization of the cells lining each abnormal lumen by immunostaining of polarity markers. As observed in 2D cultures, the apical protein gp135 and the TJ protein ZO1 showed normal localization in each lumen

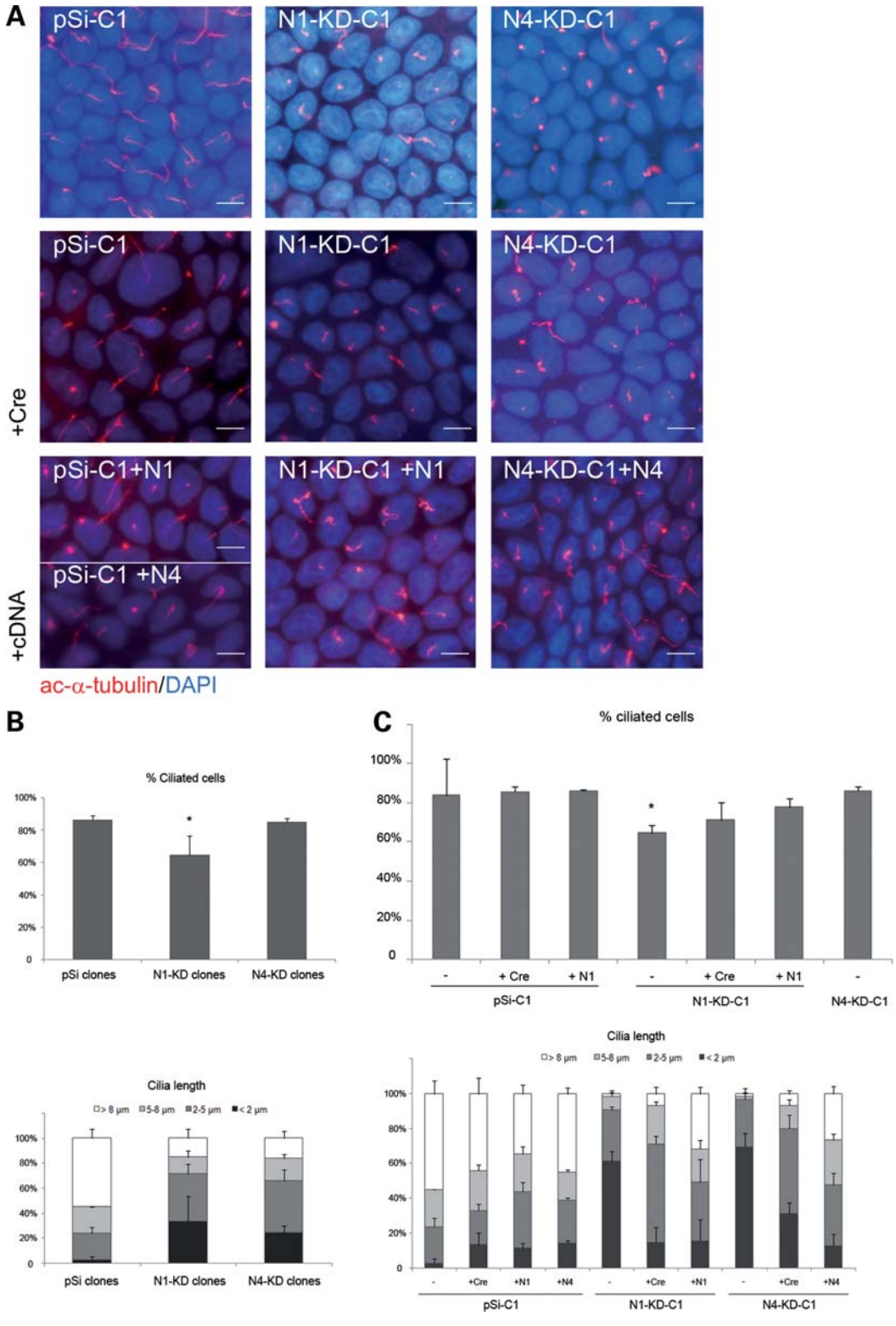

Figure 3. *NPHP* knockdown cells have abnormal cilia in 2D cultures. (**A**) Immunostaining of cilia with acetylated-α-tubulin antibody performed on MDCK cells grown on transwell filters for 7 days. Nuclei were stained with DAPI. All the results presented are obtained with the clones pSi-C1, N1-KD-C1 and N4-KD-C1 and the corresponding rescued cell lines after Cre recombination or cDNA re-expression. (**B** and **C**) Analysis of the percentage of ciliated cells (upper panel) and cilia length (lower panel) in several clonal cell lines (B) and in rescued cell lines after Cre recombination (+ Cre) or re-expression of human nephrocystin-1 (N1) or nephrocystin-4 (N4) cDNA (C). Data show the average of three different control (pSi-C1 to 3) and knockdown (N1-KD-C1, C2, C5 and N4-KD-C1, C3, C6) clonal cell lines (B). Five hundred cells of each clonal cell line were scored both for the measure of the presence and the length of the primary cilium ($P < 0.05$ compared with control cell lines, *t*-test). Scale bars are 10 μm.

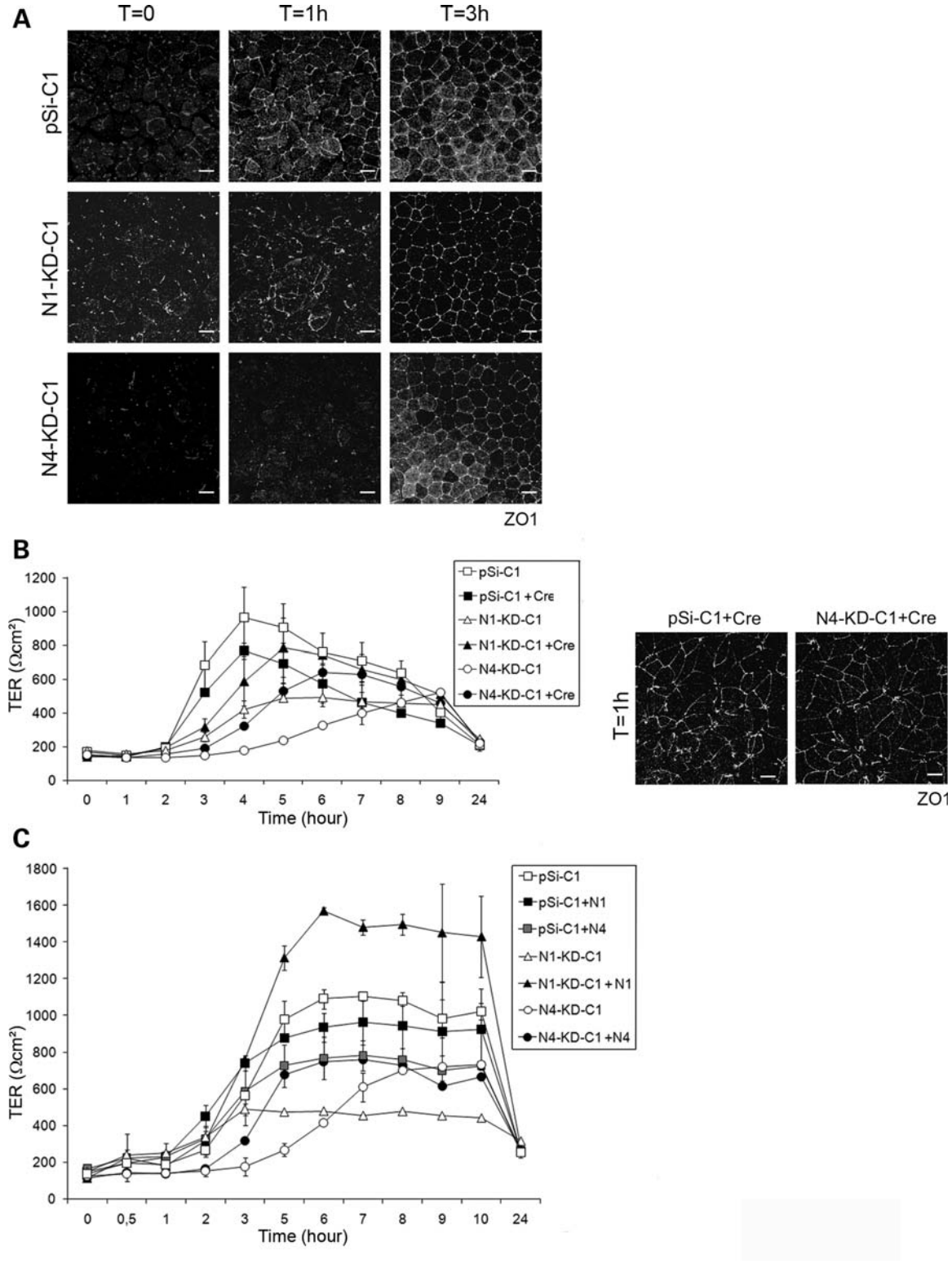

Figure 4. TJ formation is delayed in *NPHP* knockdown MDCK cells during a calcium switch experiment. Control (pSi-C1 to 3), N1-KD (N1-KD-C1, C5) and N4-KD (N4-KD-C1, C3, C6) MDCK cell lines were subjected to calcium switch experiments to assess the formation of TJs, and only data obtained with pSi-C1, N1-KD-C1 and N4-KD-C1 are shown. (**A**) Immunostaining of the TJ marker protein ZO1 at different time points after the addition of calcium (T0, 1 h, 3 h) in control and knockdown cell lines. (**B** and **C**) TER was measured hourly after calcium switch in control and knockdown (B and C), rescued Cre-infected (B) and expressing nephrocystin-1 or nephrocystin-4 cDNA (C) MDCK cell lines. Immunostaining of ZO1 protein 1 h after calcium switch is shown in rescued Cre-infected control and N4-KD clonal cell lines (B). Scale bars are 10 μm.

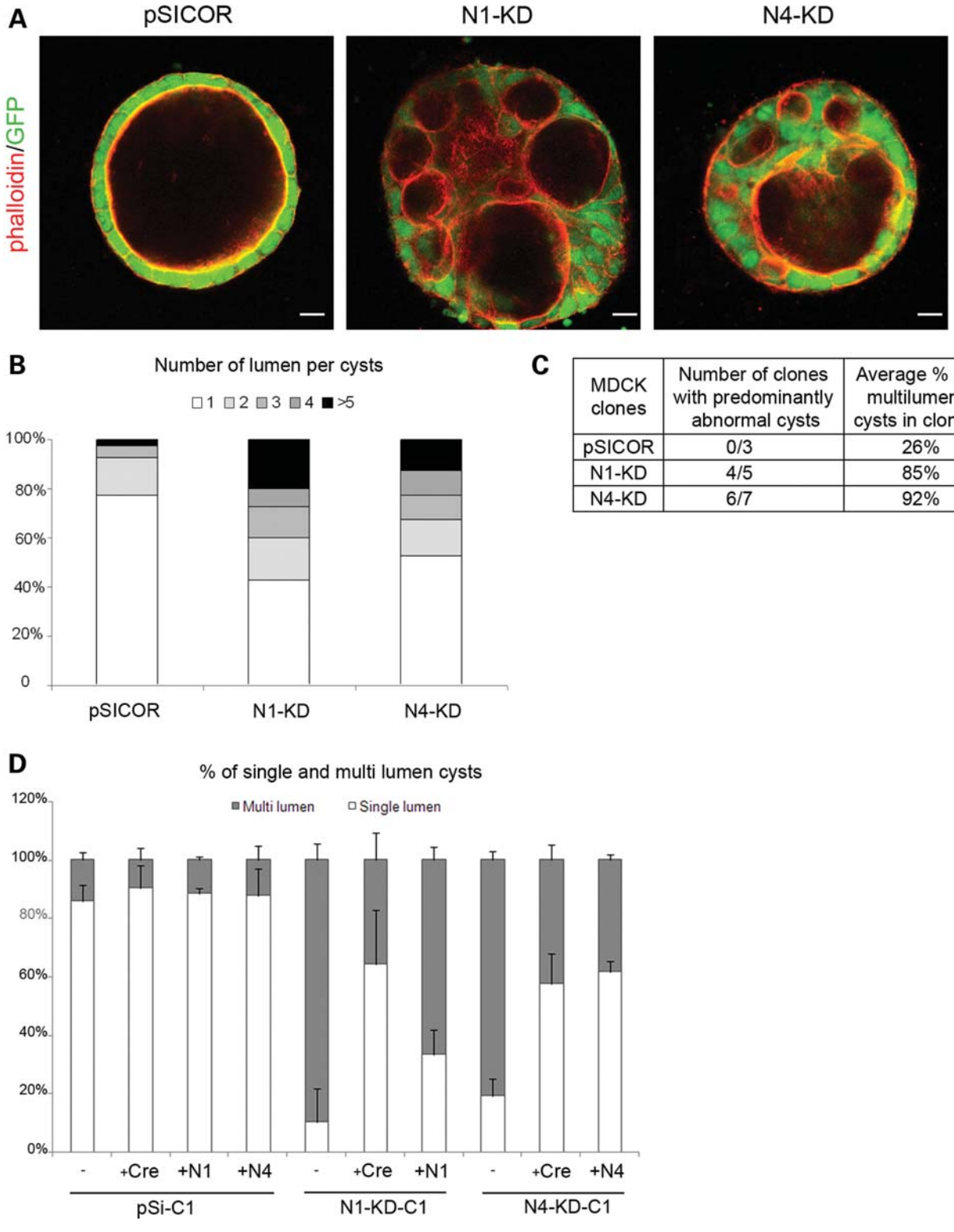

MDCK clones	Number of clones with predominantly abnormal cysts	Average % of multilumen cysts in clones
pSICOR	0/3	26%
N1-KD	4/5	85%
N4-KD	6/7	92%

Figure 5. *NPHP* knockdown MDCK cells form disorganized, multi-lumen cysts when grown in a 3D type-I collagen matrix. (**A**) Structure of the control, N1-KD and N4-KD MDCK cysts, grown for 3 weeks in type-I collagen matrix, as assessed by immunostaining of phalloidin. (**B**) Number of lumen per cysts in control, N1-KD and N4-KD polyclonal cell populations ($n = 40$). (**C**) Table summarizing the number of clones with $>50\%$ of abnormal cysts and the average percentage of multi-lumen cysts in clones. (**D**) Quantification of normal cysts in rescued Cre-infected and cDNA-re-expressing cell lines grown in 3D culture ($n = 100$). The results presented are obtained for the clones pSi-C1, N1-KD-C1 and N4-KD-C1. (**E**) Immunostainings of the apical marker gp135, the TJ marker ZO1 and the cilia marker acetylated-α-tubulin in clonal cell lines. A GFP marker is co-expressed with shRNA. Scale bars are 20 μm.

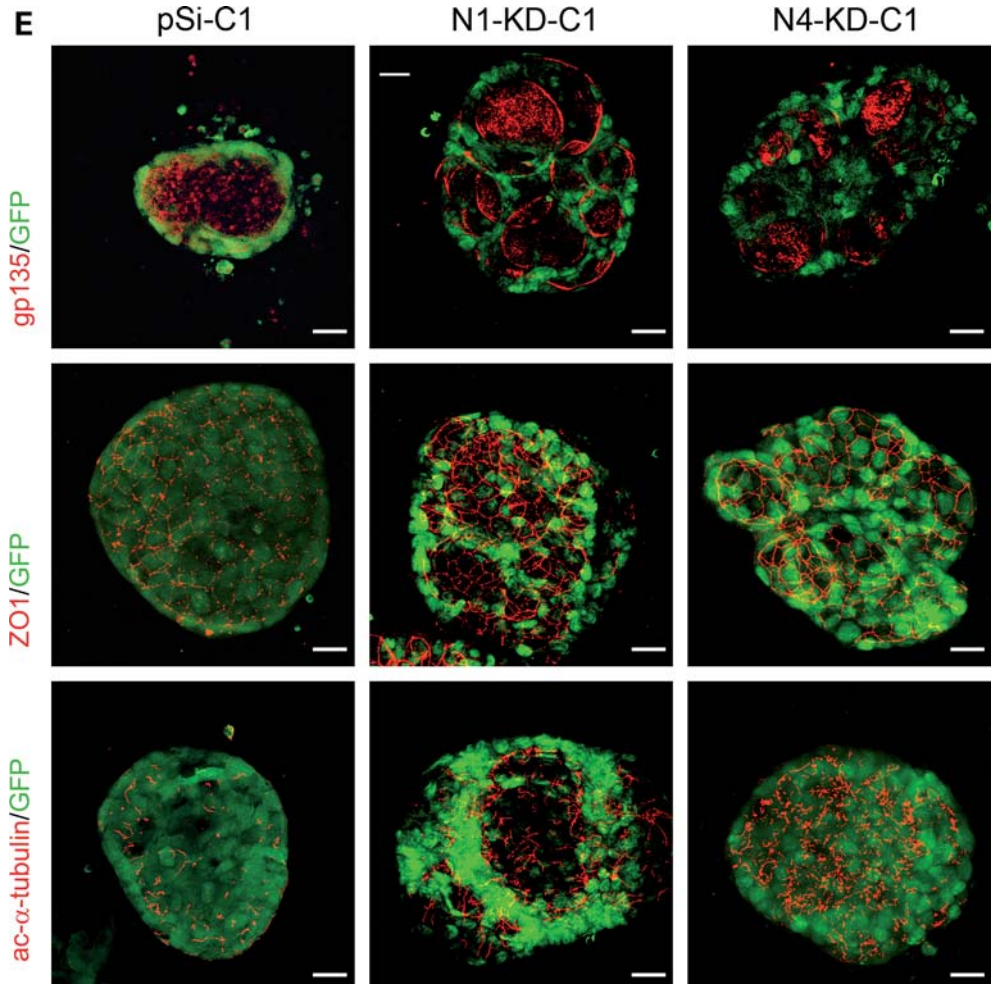

Figure 5. *Continued*

present in N1-KD and N4-KD cysts (Fig. 5E). In addition, immunostaining with acetylated-α-tubulin revealed that abnormal cysts contained apparently normal apical cilia projecting into each lumen, suggesting a correct apico-basal polarization of the cells lining each lumen. Although there was no obvious defect in the establishment of cell polarity to account for the abnormal phenotype observed in N1-KD and N4-KD cell cysts in these experiments, this does not rule out a more subtle deficit in the precise timing of TJ or polarity formation which may impair the development of proper epithelial architecture in this 3D system.

Nephrocystin proteins are associated with the polarity proteins PALS1, PATJ and Par6

Interestingly, phenotypes similar to the N1-KD and N4-KD cell lines described earlier have been reported in MDCK cell lines made deficient in the TJ protein PALS1 using shRNA knockdown (17). PALS1 is known to form a complex with CRB3 and PATJ, which, along with the Par3/Par6/aPKC complex, determines the apical domain of epithelial cells by excluding the lateral determinant Dlg/Lgl/Scrib from the apical domain (18). TJ formation was severely delayed in PALS1-deficient cell lines, and when grown in a 3D collagen matrix, these cell lines also developed abnormal structures with multiple lumens (17). We therefore hypothesized that nephrocystin function might be both structurally and functionally linked to PALS1, and to address this question, we tested whether the nephrocystins physically interact with it by performing co-immunoprecipitation assays in human embryonic kidney cells (HEK293T). Using transiently expressed PALS1-myc and either nephrocystin-1-GFP or nephrocystin-4-GFP proteins, we showed that PALS1-myc was co-immunoprecipitated with both nephrocystin-1-GFP and nephrocystin-4-GFP proteins, and these results were confirmed with the reciprocal co-immunoprecipitation (Fig. 6A and B). In addition, we showed that nephrocystin-1 was able to precipitate the PALS1 partner, PATJ (Fig. 6C). We were unable to demonstrate co-immunoprecipitation of nephrocystin-4 with PATJ since we could not achieve co-expression of both proteins in the same cells. In order to identify the regions essential for the interaction between nephrocystin-1 and PALS1, we performed GST pull-down assays. Both coiled-coil (CC) and Src homology 3 (SH3) domains of nephrocystin-1 fused to GST were sufficient to interact with PALS1. Two distinct mutations located within

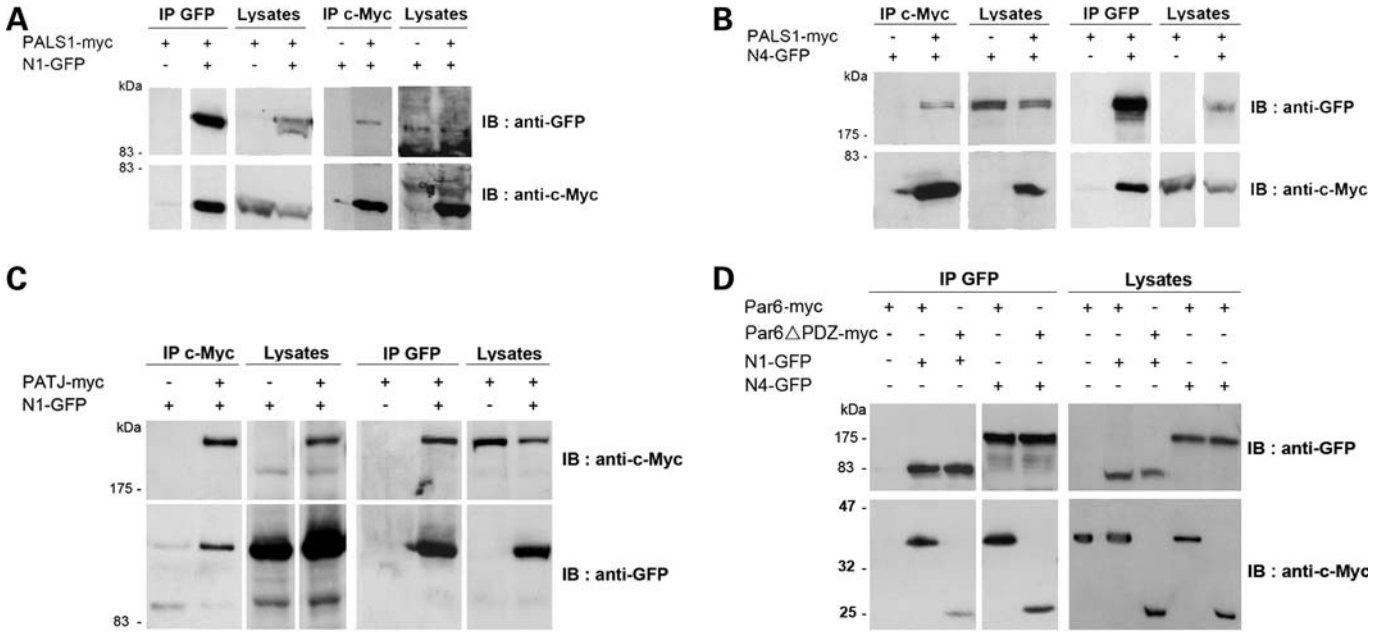

Figure 6. Characterization of the interaction of nephrocystin-1 and nephrocystin-4 with the polarity proteins PALS1, PATJ and Par6. (**A**–**D**) Co-immunoprecipitation of nephrocystin-1-GFP (N1-GFP) and nephrocystin-4-GFP (N4-GFP) with PALS1-myc (A and B), PATJ-myc (C), Par6-myc or Par6ΔPDZ-myc (D) in HEK293T cells. Lysates were immunoprecipitated with either anti-c-Myc or anti-GFP antibodies and immunoblotted with c-Myc and GFP antibodies.

the SH3 domain, p.P203L and the NPH patient mutation p.L180P, were shown to result in decreased interaction with PALS1, suggesting a possible functional significance of the nephrocystin-1/PALS1 interaction in the pathophysiology of NPH (Supplementary Material, Fig. S4). In addition, we demonstrated that a construct of nephrocystin-1 containing the CC and the SH3 regions (amino acids 1–212) was sufficient to co-immunoprecipitate PALS1 (unpublished data), indicating that the N-terminal region of nephrocystin-1 is involved in its interaction with PALS1. These results support previous data showing that MDCK cell lines stably expressing the SH3-deleted mutant of nephrocystin-1 have a reduced ability to establish TJs as measured by TER (10). As PALS1 seems to play the role of a crucial adaptor of the epithelial polarity complex at the TJ, allowing the recruitment of Par6/Par3/aPKC through the direct PALS1–Par6 interaction (17,19,20), we further investigated whether nephrocystin proteins participate in this latter interaction. Consistent with this hypothesis, overexpressed Par6-myc protein was effectively co-immunoprecipitated with both nephrocystin-1-GFP and nephrocystin-4-GFP proteins in HEK293T cells (Fig. 6D). Moreover, nephrocystin-1 and -4 interact weakly with a Par6 mutant with its PDZ domain deleted, which is known to reduce its association with PALS1 (19) or CRB3A (20), suggesting that the interaction between the nephrocystins and Par6 is dependent on PALS1 (Fig. 6D).

Immunofluorescent staining using monoclonal anti-nephrocystin-4 and polyclonal anti-PATJ or anti-ZO1 antibodies on human adult kidney sections showed that nephrocystin-4 was distributed all along the lateral cell contacts, but clearly overlapped with the endogenous PATJ and ZO1 at the TJs (Fig. 7). We also demonstrate a co-localization of nephrocystin-4 with Par3 which is known to associate with Par6 and aPKC at the TJs in human tubules (Fig. 7). Whereas PATJ, ZO1 and Par3 were ubiquitously expressed in all segments of the nephron, nephrocystin-4 was restricted to the ascending loop of Henle and distal tubules, as it co-localized with Tamm–Horsfall staining and to the collecting ducts stained with aquaporin-2 (Supplementary Material, Fig. S5). The partial overlap between the nephrocystins and these proteins at cell–cell contact regions suggests that the spatial distribution of nephrocystins may allow them to regulate TJs, which is required for proper epithelial cell morphogenesis.

DISCUSSION

Taken together, this work provides evidence for an important role for nephrocystin-1 and nephrocystin-4 in epithelial cell organization. First, the *NPHP1* and *NPHP4* genes are upregulated during cell polarization. Second, shRNA-mediated knockdown of the nephrocystins disrupts the kinetics of TJ formation during cell polarization and epithelial morphogenesis in a 3D culture system. Finally, a physical interaction with the TJ-associated proteins PALS1/PATJ complex and Par6 is demonstrated, suggesting a molecular mechanism by which these nephrocystins might participate in epithelial morphogenesis.

Alteration of nephrocystin-1 and -4 (this work) or either Par6 or PALS1 expression has strikingly similar effects on MDCK epithelial morphogenesis (17,21,22). Par6 has been shown to regulate both the loss and formation of TJs: in MDCK cells, overexpression of Par6 delays TJ assembly

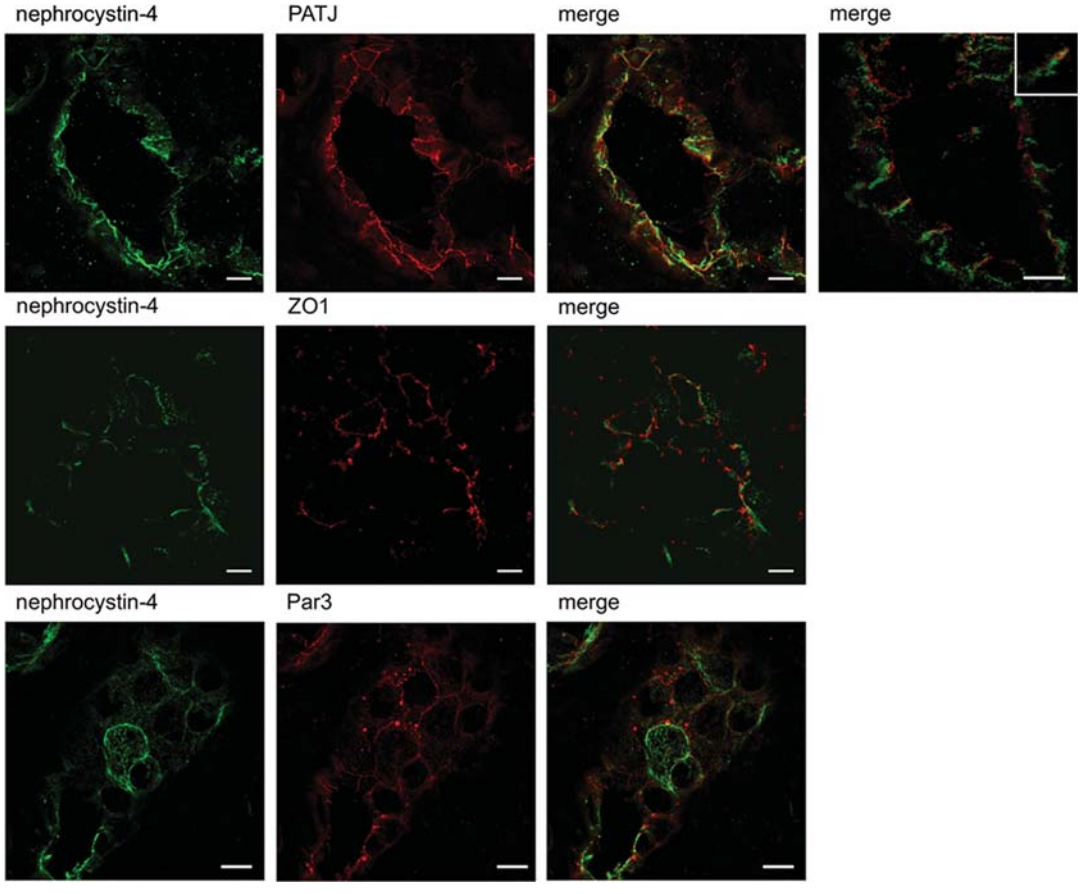

Figure 7. Partial co-localization of nephrocytin-4 and TJ markers in human renal tubules. Nephrocystin-4 (monoclonal IgG N4, green) showed partial overlap with PATJ, ZO1 and Par3 (red) localization to TJs in distal/collecting duct tubule from normal human kidney tissue. Inset shows higher magnification of a representative overlap between nephrocystin-4 and PATJ staining at the cell–cell membrane. Scale bars are 10 μm.

(21), and the expression of a dominant negative form of Par6 grown in collagen disrupts epithelial organization in 3D culture (22). Par6-dependent control of epithelial apico-basal polarity is mediated via its interactions with the CRB3A/PALS1/PATJ complex, and these two complexes cooperate to maintain one another's subcellular localization which helps define the apical membrane compartment (19). The association of nephrocystins, either directly or as a part of a multi-molecular complex linking both Crb and Par complexes, suggests that they may participate in that process, promoting the association of CRB3A/PALS1/PATJ with Par6 and thereby influencing cell polarization. An alternative explanation for nephrocystin function is that their localization at the basolateral membrane and distal TJ region could help restrict the CRB and Par complexes to the apical membrane, potentially using a microtubule-based transport mechanism, as the nephrocystins are microtubule-associated proteins. Analysis of the membrane territories of the CRB and Par complexes as well as the dynamics of these complexes in renal tubule sections of patients with mutations in either *NPHP1* or *NPHP4* genes could address this question and will be necessary to define the physiologic significance of the interaction between the nephrocystins and polarity complexes reported here.

Recently, it has been shown that polarity proteins, such as CRB3 and the Par complex, are localized not only at the TJs, but also at the primary cilium of MDCK cells (23). Par3 interacts with the anterograde intraflagellar transport (IFT) motor kinesin-2, linking polarity proteins with IFT, microtubules and the formation of cilia (23). CRB3- and Par3-knockdown MDCK cells have no or shortened cilia, respectively (23,24). This latter phenotype is similar to defects caused by extinction of *NPHP1* and *NPHP4*, suggesting that these nephrocystins may participate along with the Par polarity complex in microtubule-dependent transport during ciliogenesis.

Hence, like these polarity proteins, the nephrocystins may play a role in two separate yet linked processes: the regulation of TJ formation and cilia formation, as N1-KD and N4-KD MDCK cells exhibit defects in both processes. However, it remains possible that shortened cilium in nephrocystin-1 and -4-depleted cell lines reflects a secondary consequence of abnormal TJ formation. We noted that the defect in ciliogenesis appeared to be more severe in nephrocystin-1-depleted cell lines (which showed a defect both in cilia number and cilia length) compared with nephrocystin-4-depleted cell lines (which showed a defect only in cilia length). Similar observations have been done in *Caenorhabditis elegans*, with nphp1 mutants showing more frequent ciliary defects of

male-specific neurons than nphp4 mutants (25). Although it is tempting to speculate that nephrocystin-1 may play a more critical role in overall ciliary health than nephrocystin-4, it is difficult to make such claims in knockdown cell lines which still retain some residual protein.

NPH is somewhat unique among the spectrum of cystic kidney diseases in that interstitial fibrosis and tubular atrophy occur early in the course of disease, with cysts occurring only at a later stage and in a localized area. One speculative scenario is that defects in epithelial cell polarity could result in the acquisition of a mesenchymal phenotype, giving rise to a gradual parenchymal fibrosis and loss of renal function characteristic of this disorder. Intriguingly, PALS1 is stabilized at the TJ by a small protein, MALS3, whose knockout in mice leads to the development of hypomorphic kidneys characterized by numerous cysts and fibrosis, very similar to those seen in NPH (26). Moreover, Par6 is recruited for various signaling pathways, including TGF-β pathways, a key regulator of renal fibrosis (27). TGF-β-dependent phosphorylation of Par6 facilitates TJ dissolution and epithelial-to-mesenchymal transition in mammary gland epithelial cells (28). It remains to be determined whether nephrocystin proteins may regulate one of these pathways in tubular epithelial cells. Nonetheless, their role in epithelial polarity and formation of TJs potentially via their association with polarity proteins PALS1 and Par6 provide some clues in understanding the possible early mechanisms affected in NPH.

MATERIALS AND METHODS

Establishment of lentiviral cell lines

shRNA constructs targeting canine *NPHP1* (5′-GGTTCTCAG TAGACATGTA-3′) and *NPHP4* (5′-GCCCATCGGTG TCTACACA-3′) mRNA sequences were designed and cloned into the lentiviral pSICOR vector, kindly provided by Tyler Jacks (15), following published instructions. For lentiviral infections, human *NPHP1* and *NPHP4* cDNA cloned in pRRL.SIN.cPPT.PGK/WPRE vector (29) were modified by inserting silent shRNA-resistant mutations using site-directed mutagenesis with the following oligos (*NPHP1*: 5′-GAATGAGCATACAGGTACTGAGCCGACACGTACG-CCTCTG-3′; *NPHP4*: 5′-GCGTCAAACCTATTGGCGTCCA CTCGGTG-3′). Lentiviruses were produced in HEK239T cells, maintained in DMEM supplemented with 10% FCS, by co-transfecting pSICOR or pRRL.SIN.cPPT.PGK/WPRE constructs with pMDL, pREV and pVSVG helper vectors as described in (30). MDCK type-II cells, maintained in MEM supplemented with 10% FCS, were infected at an MOI of 20 in the presence of 8 μg/ml polybrene. For rescue experiments, pSICOR cell lines were infected by adenovirus containing the Cre recombinase gene, Ad-CMV-Cre (Vector Biolabs), at an MOI of 200.

Gene expression analysis by quantitative RT–PCR

For time-course experiments, 1×10^5 cells were seeded in six-well plates and then trypsinized at the indicated time points; for *NPHP1* and *NPHP4* gene expression in control and knockdown lines, cells were grown to confluence before being trypsinized. Total RNA was purified with a Qiagen Extraction Kit, treated with DNase I, and 1 μg of total RNA was reverse-transcribed using Superscript II (Invitrogen). Relative expression levels of the different *NPHP* mRNA were determined by real-time RT–PCR using Absolute SYBR Green ROX Mix (ABgene) and a set of primers specific for each *NPHP* gene (Supplementary Material, Table S1). *NPHP* expression performed in triplicate was normalized to *GAPDH* mRNA expression, and the data were analyzed with the $2^{-\Delta\Delta Ct}$ method using day 2 or pSICOR(−) samples as reference for time-course and knockdown experiments, respectively.

Antibodies

Antibodies used for immunofluorescence were: mouse anti-acetylated-α-tubulin, rat anti-E-cadherin, phalloidin-rhodamine (Sigma), rabbit anti-ZO1 (Zymed), mouse anti-gp135 (gift of George K. Ojakian), mouse anti-occludin (Zymed), rabbit anti-PATJ (31), rabbit anti-Par3 (Millipore) and DAPI (Vectashield HardSet Mounting Medium with DAPI). Antibodies used for immunoprecipitation and western blot were: mouse anti-GFP (Roche), anti-c-Myc (Santa Cruz), rabbit anti-α-tubulin (Invitrogen) and mouse GAPDH (Chemicon). Polyclonal anti-nephrocystin-1 (AP-N1) and anti-nephrocystin-4 (AP-N4) were previously described in Mollet *et al*. (11). Monoclonal anti-nephrocystin-4 (IgG N4) was generated from His-nephrocystin-4 fusion protein (amino acid 673–1032) produced in *Escherichia coli* SG13009 and purified by nickel affinity chromatography (Ni-NTA agarose, Qiagen). BALB/c mice were immunized with the purified nephrocystin-4 molecule, and monoclonal antibodies were generated by Biotem SARL, France (Supplementary Material, Fig. S5).

Calcium switch assay and TER measurement

MDCK cells grown on 24 mm Transwell filters for 7 days post-confluence were subjected to calcium switch as described in Straight *et al*. (17). TER was determined using a Millicell-ERS volt–ohm meter (Millipore) immediately after the addition of normal growth medium at the indicated time points.

Three-dimensional collagen gel culture

MDCK cells were trypsinized and triturated into a single-cell suspension of 1.25×10^4 cells/ml in a type-I collagen solution as described previously (32) before being plated in 48-well plates. Cultures were grown for 2–3 weeks before immunofluorescence. Lumen number analysis was performed on cell cysts grown for 2 weeks stained with phalloidin-rhodamine to visualize the lumen, and the data represent the average of 40 (polyclonal) and more than 100 (clonal) cysts per cell lines.

Immunofluorescence

MDCK cells were plated at 10^4 cells on 12 mm Transwell filter (Costar) and grew for 7 days post-confluence. Cells

were fixed in 4% paraformaldehyde in PBS for 20 min followed by treatment with 50 mM NH_4Cl for 10 min or in cold 20% methanol for 10 min (for occludin staining). Cells were then permeabilized in PBS–0.3% Triton for 3 min and treated with PBS–0.1% Tween 20–1% BSA for 10 min, before incubating with primary antibody solution for 2 h and then with appropriate fluorescent secondary antibody. Immunofluorescence labeling on adult human kidney was performed on 10 μm-thick frozen sections fixed in acetone for 10 min, treated with PBS–0.1% Tween 20–1% BSA–10% donkey serum for 1 h and incubated in the same buffer overnight at 4°C with appropriate antibodies. The number of ciliated cells and cilia length were measured using the Lucia G on Nikon DXM 1200 software (Nikon, France). Confocal images were taken using a LEICA SP5 laser scanning microscope system with an X63.2 or X40 objective (Carl Leica, Wetzlar, Germany).

Co-immunoprecipitation and GST fusion protein pull-down assays

Full-length GFP-tagged nephrocystin-1 (N1-GFP), nephrocystin-4 (N4-GFP) and GST-tagged fusion proteins corresponding to the CC domain and SH3 domain of nephrocystin-1 were previously described (7,11,33). PATJ-myc and Par6-myc constructs have been described previously (20,31), and a Par6ΔPDZ-myc construct was obtained by inserting PDZ-deleted human Par6 A/C into pcDNA3e-GFP. PALS1-myc construct was kindly provided by Ben Margolis.

N1-GFP and N4-GFP were co-transfected with PALS1-myc, PATJ-myc or Par6-myc into HEK293T cells by the calcium phosphate method. For co-immunoprecipitation assays, cells were then harvested after 2 days and lysed for 10 min with lysis buffer [1% Triton, 50 mM Tris–HCl, pH 7.5, 150 mM NaCl and 1 mM sodium orthovanadate with complete protease inhibitor cocktail (Roche Applied Science)]. Insoluble debris was removed by centrifugation at 14 000*g* for 15 min. Supernatants were incubated with the indicated antibody for 2 h, followed by 40 μl of protein A-Sepharose (Sigma) for 1 h. For GST pull-down assays, GST fusion proteins were produced in *E. coli* BL21 strain and purified using glutathione-agarose beads (Sigma). Equal amounts of GST alone and GST fusion proteins were incubated with lysates of PALS1-myc-transfected HEK293T cells for 1 h. After washes and denaturation, templates were processed for immunoblotting with the indicated antibodies.

SUPPLEMENTARY MATERIAL

Supplementary Material is available at *HMG* Online.

ACKNOWLEDGEMENTS

We thank Imane Moutkine and Rita Benkirane for technical assistance, Nicolas Goudin and Meriem Garfa-Traoré for their assistance with confocal microscopy, Philippe Moullier (Vector Core of the University Hospital, Nantes, France) for the retroviral plasmids, and Lydie Lane (Le Bivic's laboratory) for generating Par6-myc and Par6ΔPDZ-myc.

Conflict of Interest statement. None declared.

FUNDING

This work was supported by the Institut National de la Santé et de la Recherche Médicale (INSERM), the Ministère de l'Education Nationale de la Recherche et de la Technologie (MRT), the Fondation pour la Recherche Médicale (FRM, PhD grant of M.D.; S.S. is laureate of the 'Equipe FRM' grant DEQ20071210558), the Association pour l'Utilisation du Rein Artificiel (AURA) and the Agence National de la Recherche (ANR, S.S. and R.S. grant R07089KS). N.E.H. was the recipient of a Fulbright grant. A.L.B. is supported by Centre National de la Recherche Scientifique (CNRS) and by the French National Agency (ANR Crumbs) and is a 'Equipe labellisée par la Ligue Nationale contre le Cancer'. Funding to pay the Open Access publication charges for this article was provided by Université Paris Descartes.

REFERENCES

1. Bisgrove, B.W. and Yost, H.J. (2006) The roles of cilia in developmental disorders and disease. *Development*, **133**, 4131–4143.
2. Otto, E.A., Schermer, B., Obara, T., O'Toole, J.F., Hiller, K.S., Mueller, A.M., Ruf, R.G., Hoefele, J., Beekmann, F., Landau, D. *et al.* (2003) Mutations in INVS encoding inversin cause nephronophthisis type 2, linking renal cystic disease to the function of primary cilia and left-right axis determination. *Nat. Genet.*, **34**, 413–420.
3. Olbrich, H., Fliegauf, M., Hoefele, J., Kispert, A., Otto, E., Volz, A., Wolf, M.T., Sasmaz, G., Trauer, U., Reinhardt, R. *et al.* (2003) Mutations in a novel gene, NPHP3, cause adolescent nephronophthisis, tapeto-retinal degeneration and hepatic fibrosis. *Nat. Genet.*, **34**, 455–459.
4. Mollet, G., Salomon, R., Gribouval, O., Silbermann, F., Bacq, D., Landthaler, G., Milford, D., Nayir, A., Rizzoni, G., Antignac, C. *et al.* (2002) The gene mutated in juvenile nephronophthisis type 4 encodes a novel protein that interacts with nephrocystin. *Nat. Genet.*, **32**, 300–305.
5. Roepman, R., Letteboer, S.J., Arts, H.H., van Beersum, S.E., Lu, X., Krieger, E., Ferreira, P.A. and Cremers, F.P. (2005) Interaction of nephrocystin-4 and RPGRIP1 is disrupted by nephronophthisis or Leber congenital amaurosis-associated mutations. *Proc. Natl Acad. Sci. USA*, **102**, 18520–18525.
6. Bergmann, C., Fliegauf, M., Bruchle, N.O., Frank, V., Olbrich, H., Kirschner, J., Schermer, B., Schmedding, I., Kispert, A., Kranzlin, B. *et al.* (2008) Loss of nephrocystin-3 function can cause embryonic lethality, Meckel–Gruber-like syndrome, situs inversus, and renal-hepatic-pancreatic dysplasia. *Am. J. Hum. Genet.*, **82**, 959–970.
7. Delous, M., Baala, L., Salomon, R., Laclef, C., Vierkotten, J., Tory, K., Golzio, C., Lacoste, T., Besse, L., Ozilou, C. *et al.* (2007) The ciliary gene RPGRIP1L is mutated in cerebello-oculo-renal syndrome (Joubert syndrome type B) and Meckel syndrome. *Nat. Genet.*, **39**, 875–881.
8. Benzing, T., Gerke, P., Hopker, K., Hildebrandt, F., Kim, E. and Walz, G. (2001) Nephrocystin interacts with Pyk2, p130(Cas), and tensin and triggers phosphorylation of Pyk2. *Proc. Natl Acad. Sci. USA*, **98**, 9784–9789.
9. Donaldson, J.C., Dempsey, P.J., Reddy, S., Bouton, A.H., Coffey, R.J. and Hanks, S.K. (2000) Crk-associated substrate p130(Cas) interacts with nephrocystin and both proteins localize to cell–cell contacts of polarized epithelial cells. *Exp. Cell Res.*, **256**, 168–178.
10. Donaldson, J.C., Dise, R.S., Ritchie, M.D. and Hanks, S.K. (2002) Nephrocystin-conserved domains involved in targeting to epithelial cell–cell junctions, interaction with filamins, and establishing cell polarity. *J. Biol. Chem.*, **277**, 29028–29035.
11. Mollet, G., Silbermann, F., Delous, M., Salomon, R., Antignac, C. and Saunier, S. (2005) Characterization of the nephrocystin/nephrocystin-4

complex and subcellular localization of nephrocystin-4 to primary cilia and centrosomes. *Hum. Mol. Genet.*, **14**, 645–656.
12. Nurnberger, J., Bacallao, R.L. and Phillips, C.L. (2002) Inversin forms a complex with catenins and *N*-cadherin in polarized epithelial cells. *Mol. Biol. Cell*, **13**, 3096–3106.
13. Stein, M., Wandinger-Ness, A. and Roitbak, T. (2002) Altered trafficking and epithelial cell polarity in disease. *Trends Cell Biol.*, **12**, 374–381.
14. Fliegauf, M., Horvath, J., von Schnakenburg, C., Olbrich, H., Muller, D., Thumfart, J., Schermer, B., Pazour, G.J., Neumann, H.P., Zentgraf, H. *et al.* (2006) Nephrocystin specifically localizes to the transition zone of renal and respiratory cilia and photoreceptor connecting cilia. *J. Am. Soc. Nephrol.*, **17**, 2424–2433.
15. Ventura, A., Meissner, A., Dillon, C.P., McManus, M., Sharp, P.A., Van Parijs, L., Jaenisch, R. and Jacks, T. (2004) Cre-lox-regulated conditional RNA interference from transgenes. *Proc. Natl Acad. Sci. USA*, **101**, 10380–10385.
16. McAteer, J.A., Evan, A.P. and Gardner, K.D. (1987) Morphogenetic clonal growth of kidney epithelial cell line MDCK. *Anat. Rec.*, **217**, 229–239.
17. Straight, S.W., Shin, K., Fogg, V.C., Fan, S., Liu, C.J., Roh, M. and Margolis, B. (2004) Loss of PALS1 expression leads to tight junction and polarity defects. *Mol. Biol. Cell*, **15**, 1981–1990.
18. Shin, K., Fogg, V.C. and Margolis, B. (2006) Tight junctions and cell polarity. *Annu. Rev. Cell Dev. Biol.*, **22**, 207–235.
19. Hurd, T.W., Gao, L., Roh, M.H., Macara, I.G. and Margolis, B. (2003) Direct interaction of two polarity complexes implicated in epithelial tight junction assembly. *Nat. Cell Biol.*, **5**, 137–142.
20. Lemmers, C., Michel, D., Lane-Guermonprez, L., Delgrossi, M.H., Medina, E., Arsanto, J.P. and Le Bivic, A. (2004) CRB3 binds directly to Par6 and regulates the morphogenesis of the tight junctions in mammalian epithelial cells. *Mol. Biol. Cell*, **15**, 1324–1333.
21. Gao, L., Joberty, G. and Macara, I.G. (2002) Assembly of epithelial tight junctions is negatively regulated by Par6. *Curr. Biol.*, **12**, 221–225.
22. Kim, M., Datta, A., Brakeman, P., Yu, W. and Mostov, K.E. (2007) Polarity proteins PAR6 and aPKC regulate cell death through GSK-3beta in 3D epithelial morphogenesis. *J. Cell Sci.*, **120**, 2309–2317.
23. Fan, S., Hurd, T.W., Liu, C.J., Straight, S.W., Weimbs, T., Hurd, E.A., Domino, S.E. and Margolis, B. (2004) Polarity proteins control ciliogenesis via kinesin motor interactions. *Curr. Biol.*, **14**, 1451–1461.
24. Sfakianos, J., Togawa, A., Maday, S., Hull, M., Pypaert, M., Cantley, L., Toomre, D. and Mellman, I. (2007) Par3 functions in the biogenesis of the primary cilium in polarized epithelial cells. *J. Cell Biol.*, **179**, 1133–1140.
25. Jauregui, A.R., Nguyen, K.C., Hall, D.H. and Barr, M.M. (2008) The *Caenorhabditis elegans* nephrocystins act as global modifiers of cilium structure. *J. Cell Biol.*, **180**, 973–988.
26. Olsen, O., Funke, L., Long, J.F., Fukata, M., Kazuta, T., Trinidad, J.C., Moore, K.A., Misawa, H., Welling, P.A., Burlingame, A.L. *et al.* (2007) Renal defects associated with improper polarization of the CRB and DLG polarity complexes in MALS-3 knockout mice. *J. Cell Biol.*, **179**, 151–164.
27. Bottinger, E.P. (2007) TGF-beta in renal injury and disease. *Semin. Nephrol.*, **27**, 309–320.
28. Ozdamar, B., Bose, R., Barrios-Rodiles, M., Wang, H.R., Zhang, Y. and Wrana, J.L. (2005) Regulation of the polarity protein Par6 by TGFbeta receptors controls epithelial cell plasticity. *Science*, **307**, 1603–1609.
29. Zufferey, R., Dull, T., Mandel, R.J., Bukovsky, A., Quiroz, D., Naldini, L. and Trono, D. (1998) Self-inactivating lentivirus vector for safe and efficient *in vivo* gene delivery. *J. Virol.*, **72**, 9873–9880.
30. Dull, T., Zufferey, R., Kelly, M., Mandel, R.J., Nguyen, M., Trono, D. and Naldini, L. (1998) A third-generation lentivirus vector with a conditional packaging system. *J. Virol.*, **72**, 8463–8471.
31. Lemmers, C., Medina, E., Delgrossi, M.H., Michel, D., Arsanto, J.P. and Le Bivic, A. (2002) hINADl/PATJ, a homolog of discs lost, interacts with crumbs and localizes to tight junctions in human epithelial cells. *J. Biol. Chem.*, **277**, 25408–25415.
32. Pollack, A.L., Runyan, R.B. and Mostov, K.E. (1998) Morphogenetic mechanisms of epithelial tubulogenesis: MDCK cell polarity is transiently rearranged without loss of cell–cell contact during scatter factor/hepatocyte growth factor-induced tubulogenesis. *Dev. Biol.*, **204**, 64–79.
33. Le Maire, A., Weber, T., Saunier, S., Broutin, I., Antignac, C., Ducruix, A. and Dardel, F. (2005) Solution NMR structure of the SH3 domain of human nephrocystin and analysis of a mutation-causing juvenile nephronophthisis. *Proteins*, **59**, 347–355.